Cytometry PART A
Journal of the International Society for Advancement of Cytometry

MIFlowCyt

Advanced Consumable-Free Morphological Analysis of Intact Red Blood Cells by a Compact Scanning Flow Cytometer

K.V. Gilev,[1,2] E.S. Yastrebova,[1,2] D.I. Strokotov,[1,3] M.A. Yurkin,[1,2] N.A. Karmadonova,[4] A.V. Chernyshev,[1,2] V.V. Lomivorotov,[4] V.P. Maltsev[1,2,3]*

[1]Voevodsky Institute of Chemical Kinetics and Combustion SB RAS, Institutskaya 3, Novosibirsk 630090, Russia

[2]Novosibirsk State University, Pirogova 2, Novosibirsk 630090, Russia

[3]Novosibirsk State Medical University, Krasny Prospect 52, Novosibirsk 630091, Russia

[4]Siberian Biomedical Research Center, Rechkunovskaya 15, Novosibirsk 630055, Russia

Received 26 October 2017; Revised 27 February 2017; Accepted 2 May 2017

Grant sponsor: Russian Science Foundation, Grant number: 17-75-30008

Grant sponsor: Russian Foundation for Basic Research, Grant number: 16-34-00476 (excluding fabrication of optical cuvette covered)

Grant sponsor: Stipend of the President of Russian Federation for young scientists (D.I.S)

Additional Supporting Information may be found in the online version of this article

*Correspondence to: Professor Valeri P. Maltsev, Voevodsky Institute of Chemical Kinetics and Combustion SB RAS, Institutskaya 3, Novosibirsk, 630090, Russia
Email: maltsev@kinetics.nsc.ru

Published online 19 May 2017 in Wiley Online Library (wileyonlinelibrary.com)

DOI: 10.1002/cyto.a.23141

ISAC
International Society for Advancement of Cytometry

Abstract

Whereas modern automated blood cell analyzers measure the volume of individual red blood cells (RBCs), leading to four RBC indices (mean corpuscular volume, MCV; mean corpuscular hemoglobin, MCH; mean corpuscular hemoglobin concentration, MCHC; red cell distribution width, and RDW), the RBC shape has not been assessed by clinical screening tools. We applied the scanning flow cytometer (SFC) for complete characterization of intact RBC morphology in terms of diameter, maximal and minimal thicknesses, volume, surface area, sphericity index, spontaneous curvature, hemoglobin concentration, and content. The above-mentioned individual RBC characteristics were measured without fluorescent markers and other chemicals by a SFC equipped only with 660 nm laser for RBC illumination and single detector for measurement of angle-resolved light scattering. The distributions over all RBC characteristics were constructed and processed statistically to form the novel 31 RBC indices for 22 donor samples. Our results confirm the possibility of precise, label-free, enhanced morphological analysis of individual intact RBCs with compact single-detector flow cytometer. Detailed characterization of RBCs with high statistics and precision can be used to increase the value of screening examinations and to reveal pathologies accompanied by abnormality of RBC shape. © 2017 International Society for Advancement of Cytometry

Key terms

cell shape; flow cytometry; light scattering; membrane curvature; red blood cells

Introduction

Counting red blood cells (RBCs) and determination of such characteristics as volume, shape, and hemoglobin concentration allows one to assess blood status and to reveal a number of diseases such as anemia, hereditary spherocytosis, hereditary elliptocytosis, sickle cells disease, and myeloproliferative disorders (1,2). Manual observation and counting of cells by light microscopy is widely used for RBC characterization (3). In spite of insufficient accuracy and impossibility to measure hemoglobin concentration, this method is routinely used for clinical blood analysis, specifically for detection and characterization of abnormal cells, which cannot be treated with automatic methods. There are improved devices that automatically scan RBCs in microcapillaries and micropipettes and perform size determination, but the cell shape can be deformed by the capillary itself (4–6).

A number of methods described in research papers do allow measuring volume, shape, and hemoglobin content (refractive index, RI) of individual RBCs, including interference microscopy (7), digital holographic microscopy (8,9), dielectric spectroscopy (10), confocal microscopy (11), quantitative phase, and amplitude microscopy (12), transillumination microscopy (13), and diffraction optical tomography

(14,15). However, they are based on time-consuming and expensive techniques and are not yet ready for high-throughput applications, such as routine clinical blood testing. Nowadays, only two approaches for RBC characterization—impedance method (Coulter principle) (16) and two-angle scattering (17)—are implemented commercially.

Automatic counting and volume measurement of RBCs is commonly performed with the impedance method (16,18). In spite of statistically significant number of measured RBCs in a flow cuvette, it ignores shape and hemoglobin-concentration differences between measured cells introducing uncontrolled errors. The impedance method measures the volume of single RBC only and allows one to evaluate the mean corpuscular volume (MCV) and red cell distribution width (RDW). The mean corpuscular hemoglobin (MCH) and mean corpuscular hemoglobin concentration (MCHC) are evaluated from additional measurement of optical density (hemoglobin absorption) of blood sample where RBCs have been lysed.

A similar technique is the flow cytometry, based on measurement of light scattering by single cells, in most cases—forward and side scattering. The main limitation of existing instruments is the need to spherize RBCs prior to their characterization. This requires additional probe preparation, and only the cell volume, but not the shape can be estimated (17,19). There were some attempts to assess deformation of RBCs within flow cytometry approach (20) and coupled with imaging technique (21), but it led only to qualitative results.

A promising approach for complete and rapid characterization of RBCs is the scanning flow cytometry (SFC), based on measuring of a larger amount of light-scattering information from each cell in a flow (22,23). Specifically, light scattering profile (LSP) is measured in a wide range of scattering angles. The core of the characterization method is the solution of the inverse light-scattering (ILS) problem, using a parametric shape model of the characterized particle (24,25). This approach has been successfully applied to RBCs (26,27), as well as to other biological particles, including platelets, bacteria, blood microparticles, and milk fat globules (24,28–31). Conceptually similar approach, based on LSP measurement combined with fitting theoretical LSPs, has been recently demonstrated for determination of RBC diameters in a microfluidic channel (32). This method showed weak agreement between experiment and theory, ignoring shape and hemoglobin-concentration differences between measured cells, and introduced undefined systematical bias into the estimation of individual RBC diameters.

Powered by the approach introduced in our recent article (27) we analyzed RBCs of 22 donors utilizing the SFC with neither fluorescent markers nor other chemicals. Specifically, RBC analysis is implemented with a 660 nm laser for RBC illumination and single photomultiplier tube (PMT) for measurement of LSPs. Such compact SFC can be incorporated into hematological analyzer to provide detailed analysis of RBC morphology in practical medicine.

Materials and Methods

Blood Samples

The local ethics committee of Siberian Biomedical Research Center approved this study. After written informed consent, blood samples were taken from 22 healthy donors by venipuncture and collected in a 2 mL vacuum tube containing EDTA as anticoagulant. The five microliters of blood from the tube were 1000-fold diluted in 0.9% saline and measured with the SFC. 4 μm polystyrene microspheres (Molecular Probes, USA) were added for SFC initialization. All measurements were performed at room temperature (22°C). >1,000 cells were measured for each donor (exact values can be found in online Supporting Information, last row).

Flow Cytometer

Technical features of the SFC and the operational function of the optical cell were previously described in detail elsewhere (22,23). The SFC was fabricated by Cytonova LLC. (Novosibirsk, Russia). The current SFC is equipped by a 40 mW laser of 660 nm (LM-660–20-S) for illumination of individual cells. The laser beam passing through the hole in the mirror illuminates a cell in the capillary from the right side of the optical cuvette (Fig. 1a). Hydrofocused cell-carrying flow is directed into the capillary from the left side of the optical cuvette—a quartz cylinder capped by a hemisphere. The surface of the hemisphere is coated by protected aluminium and reflects light scattered by a cell back to the pierced mirror and further to the lens focusing it on a diaphragm in front of a PMT (Fig. 1a). The operational angular range for scattering angle θ of the SFC was determined from the analysis of polystyrene microspheres (29) to be from 10° to 60°. In the current experiments the RBCs were measured with an average rate of 200 cells per second.

Data Processing

The measured LSPs of each cell were processed using the optical model of an intact RBC (Fig. 1b) and solution of the ILS problem as described in our recent article (27). This approach is based on the preliminary calculated database of theoretical LSPs and does not require any calibration procedure for determination of absolute characteristics of RBC. The polystyrene microspheres were used only in initialization of the SFC to determine a quality of optical alignment through the fitting of experimental LSP of a single microsphere by the LSPs calculated from the Mie theory. The fit provides us with size and refractive index of the microsphere, flow speed, and normalization coefficient between theory and experiment. The "perfect" alignment corresponds to 10 nm precision in sizing of microsphere.

The five characteristics provide complete description of a RBC optical model which are as follows: diameter d, maximal thickness h_{max} and minimal thickness h_{min} (geometrical), refractive index RI (structural) and orientation angle β between the direction of the laser beam and the RBC symmetry axis (positional). The geometrical characteristics of the RBC shape model are shown in Fig. 1b). Since a RBC contains no nucleus and its membrane width is much smaller than the

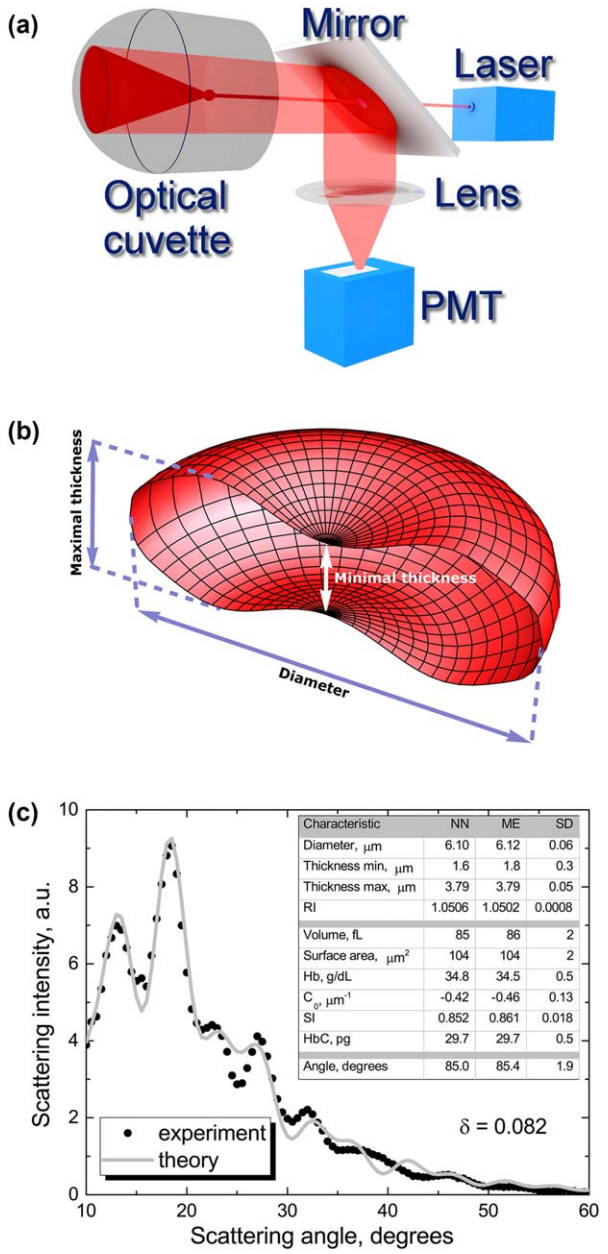

Figure 1. (**a**) Schematic layout of optical part of the scanning flow cytometer. (**b**) Optical model of a RBC, showing the main geometrical characteristics. (**c**) Typical result of processing of single LSP of individual RBC measured with the SFC. Values of nearest neighbor (NN), mathematical expectation (ME), and standard deviation (SD) are shown for retrieved characteristics of the RBC. The quantity δ indicates the degree of agreement between experiment and theory. [Color figure can be viewed at wileyonlinelibrary.com]

wavelength, it can be considered as a homogenous body with RI determined solely by the hemoglobin concentration. The RBC shape model is based on minimization of bending energy of the membrane with isotropic elasticity, for which analytical approximation was previously constructed (27). Compared to that study, we had to substantially expand the database of theoretical LSPs to cover all possible variations in RBC characteristics of different donors. The current database contains 605,000 entries with RBC characteristics randomly distributed in the following intervals: d from 4.0 μm to 10.01 μm; h_{min}, from 0.01 μm to 7.0 μm; h_{max}, from 1.3 μm to 7.0 μm; RI from 1.385 to 1.43; β from 70° to 90°. The interval for β is determined by the hydrofocusing effect orienting oblate particles along a maximal dimension in Poiseuille flow. This effect was analyzed both theoretically (22) and in experiments with SFC (26). Additionally we have applied the constraints based on the data by Fung et al. (7): $h_{min} \le h_{max}$, $V \in [35,168]$ fl, SI$\in[0.55,1]$. Sphericity index $SI = 3(4\pi)^{1/2}VS^{-3/2}$ is a ratio of the RBC volume V to the volume of a sphere with the same surface area S; it is equal to 1 for spherical particles. For each RBC from the database we calculated the theoretical LSP using the ADDA code v.1.2 (33) at the Supercomputing center of the Novosibirsk State University. Based on the Bayesian approach (25), the characterization method provides the following values for each cellular characteristic: nearest neighbor in database (NN or best-fit), mathematical expectation (ME), and standard deviation (SD). Typical result of LSP processing is shown in Fig. 1c). This analysis takes approximately 0.25 s at single core of 2.4 MHz Intel processor per a cell. Experimental and theoretical LSPs were multiplied by the weighting function $w(\theta) = (1°/\theta)\exp[-2\ln^2(\theta/54°)]$ which is an approximation of the SFC transfer function and provides an uniform experimental-noise level over the considered angular region (24). Here the scattering intensity is given in arbitrary units, but it can be easily transformed into the differential light-scattering cross section (34).

Results

The determined RBC characteristics may be divided into three categories: morphological, structural, and positional (inset in Fig. 1c). In general, all RBC characteristics have to be introduced in the following form: ME $\pm$ SD. For example, the diameter of the RBC shown in Fig. 1c) is 6.12 $\pm$ 0.06 μm. The angle β is a positional characteristic—it affects the LSP, but has no biological relevance. The diameter, maximal and minimal thicknesses form the primary morphological set, from which other morphological values, namely V, S, SI, spontaneous curvature c_0, can be calculated, see (27) for a detailed procedure. The RI is the primary structural characteristic, from which the hemoglobin concentration (Hb) and content (HbC) in individual RBCs are calculated using the molar refractivity formula (17,35). Moreover, we introduced the additional characteristic of RBC morphology—dimensionless spontaneous curvature c_d, scaled by the curvature of the surface-equivalent sphere:

$$c_d = c_0\left(\frac{S}{4\pi}\right)^{1/2} = c_0\left(\frac{3V}{4\pi \cdot SI}\right)^{1/3}, \quad (1)$$

which together with SI determines the dimensionless shape of the RBC, similarly to h_{min}/d and h_{max}/d as discussed in Ref. (27).

The quality of fit of each experimental LSP can be assessed by the degree of agreement δ, defined as root mean square difference between experimental and best-fit

Table 1. The RBC indices for donor #21.

CHARACTERISTIC	MEAN	SD	SKEWNESS
Diameter, μm	6.490	0.763	0.44
Min thickness, μm	1.933	0.892	0.19
Max thickness, μm	3.122	0.474	0.64
Volume, fl	82.2	21.6	0.62
Surface, μm^2	104.3	20.4	0.58
Sphericity index	0.816	0.082	−0.26
Spontaneous curvature, μm^{-1}	−0.502	0.292	−0.38
Dimensionless spontaneous curvature	−1.361	0.732	0.08
Hb concentration, g/dL	38.11	4.96	0.01
Hb content, pg	30.06	6.73	0.64
Median δ		0.111	

theoretical weighted LSPs divided by root mean square of experimental one. In particular, the δ for theoretical and experimental LSPs shown in Figure 1c is 8.2% that corresponds to a near-perfect agreement. This results in subdiffraction precision (SD in Fig. 1c) of main RBC morphological characteristics, namely, 60 and 50 nm for diameter and maximal thickness, respectively. The minimal thickness is determined with diffraction resolution, because the LSP is less sensitive to this characteristic. The latter follows both from theoretical simulations (fixing all other characteristics and varying the minimal thickness—data not shown) and from the obtained uncertainties during processing experimental LSPs in Ref. (27).

Based on analysis of individual LSPs, we performed statistical processing of distributions over RBC characteristics of 22 donors. In addition to mean values and standard deviations, we decided to show distribution skewness acknowledging the asymmetry of corresponding distributions, since it demonstrated a strong variations from donor to donor. This processing allowed us to determine 31 RBC indices for each donor formed by mean, SD and skewness of the distributions and median δ. The RBC indices of all donors can be found in the online Supporting Information. In particular, the RBC indices of the donor #21 are very close to average values over all analyzed donors and we have summarized them in Table 1. We do not show the standard errors of means for all indices in the Table 1 to prevent over-digitizing view of the data. In fact, the standard error of mean of the certain RBC index does not exceed a few units of the last significant digit of the value, for example, the mean diameter of RBCs for donor #21 is 6.490 ± 0.011 μm. The means, SDs and median δ for all donors are graphically shown in Figure 2. We empirically divided the median δ plot in three parts colored in shades of gray. The near-perfect agreement corresponds to $\delta < 0.09$. The δ that falls into range 0.09–0.12 relates to good agreement between experiment and theory. The δ that exceeds 0.12 can be associated with poor one.

Our measurements of RBC characteristics allow us to construct scatterplots for best visual analysis of results. For example, three scatterplots for donor #21 are shown in Figure 3 (left column). The thickness-versus-diameter scatterplot allows one to identify non-standard cells, such as top tail, associated with almost spherical RBCs, for example, reticulocytes. This fact requires additional study with simultaneous measurement of LSP and fluorescence to detect RNA in cells. The surface-versus-volume scatterplot forms a narrow band, which is expected from consideration of RBC transit through very thin blood vessels, capillaries (3). The sphericity-index-versus-volume scatterplot demonstrates variability of RBC shapes in population. To demonstrate the variability of scatterplots from donor to donor we show the same scatterplots for donor #5 in Figure 3 (right column). All of them are significantly different from donor #21 counterparts. Most visible

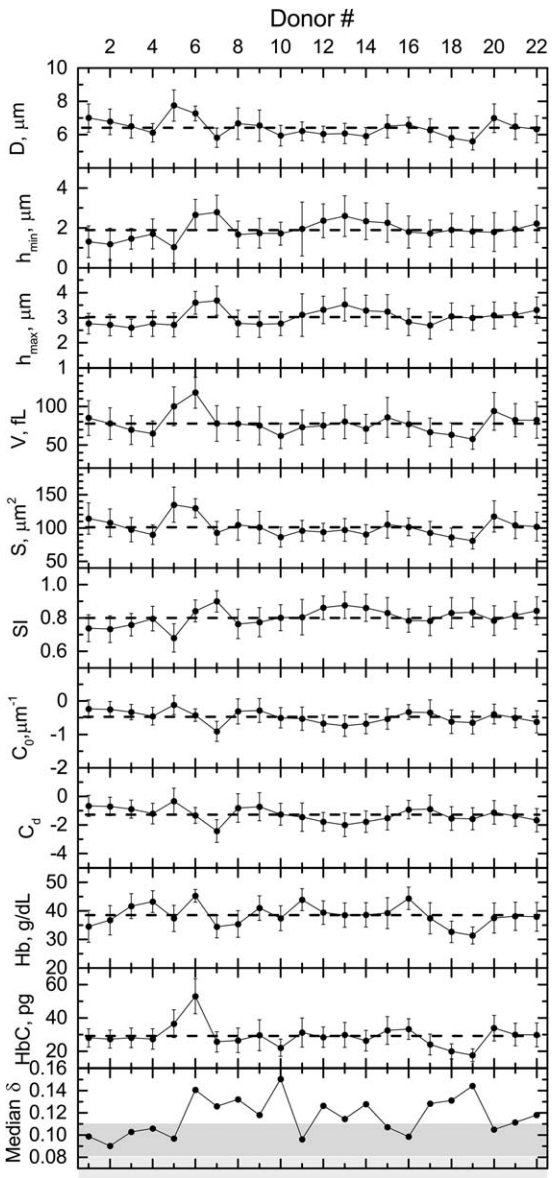

Figure 2. Mean over sample values and standard deviations (shown as error bars) for RBC indices of 22 donors. The last row shows median over sample δ.

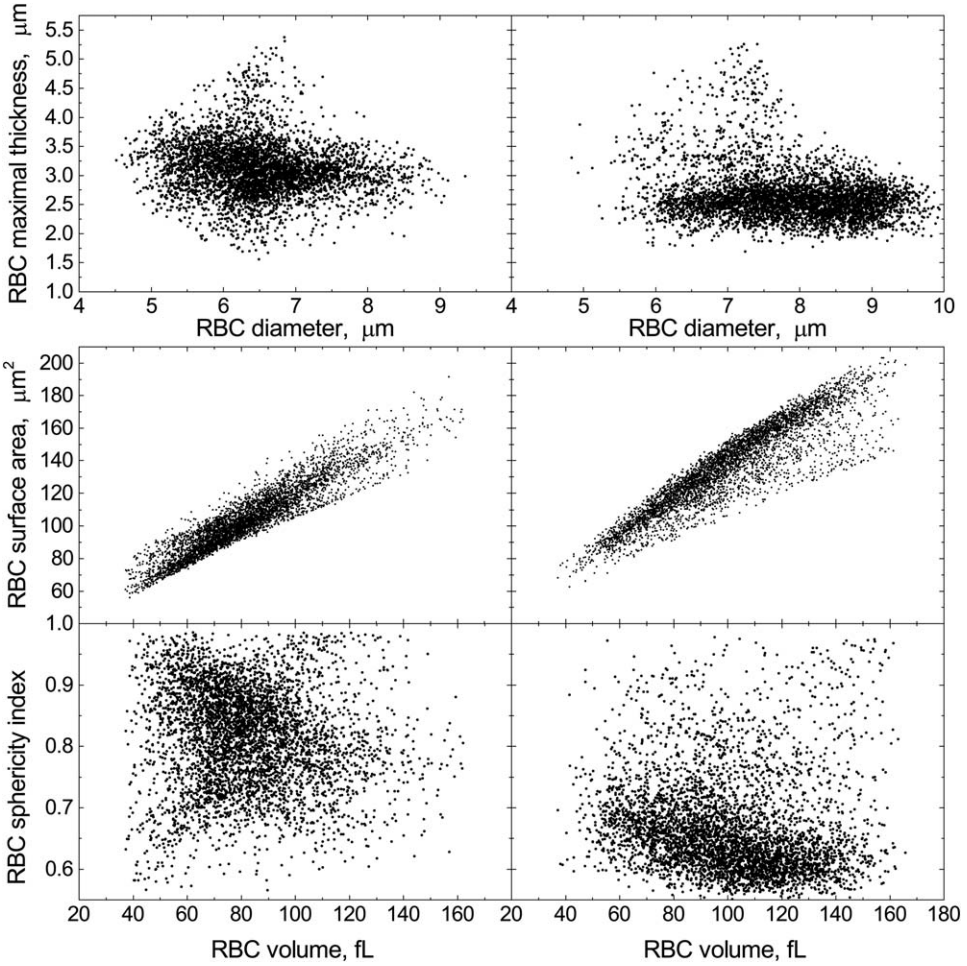

Figure 3. Scatterplots of RBC characteristics for donor #21 (left column) and #5 (right column).

is the difference in sphericity-index-versus-volume scatterplot that reflects larger oblateness of RBCs of donor #5.

Even more detailed visual analysis of the obtained RBC characteristics can be performed with the help of 3D scatterplots. For example, the 3D scatterplot (sphericity index versus volume versus diameter) for donor #21 is shown in Figure 4. Obviously, 3D scatterplot should be visualized on gadget monitors with rotation options. It may be useful in constructing of a qualitative result of analysis whereas a quantitative result can be formed from an analysis of 31 indices, for example, Table 1.

Finally, we summarize the results of RBC indices (mean values) for all donors, by showing the minimal, average, and maximal means in Table 2.

Discussion

The current SFC design resulting in compact optical scheme with only a single laser and a PMT allows measurement of LSPs from individual intact RBCs in a flow. Coupled with the solution of the ILS problem this leads to the detailed characterization of every cell. We determine primary characteristics—diameter, maximal and minimal thicknesses, refractive index—with high accuracy and further calculate several derived ones: volume, surface area, sphericity index, spontaneous curvature, dimensionless spontaneous curvature, and hemoglobin concentration and content. Contrary to the impedance method and ordinary light-scattering flow cytometry the scanning flow cytometry provides determination of errors for all measured characteristics, defining the new metrological level in RBC characterization. Moreover, these errors may play an important role in identification of abnormal cells in blood. Finally, 31 RBC indices (Table 1) of each patient can be measured with the SFC contrary to four RBC indices currently available with automated hematology analyzers (36). All RBC indices measured with the new method for 22 donors showed variations from donor to donor in reasonable physiological ranges.

The quality of analysis, that is, averaged fit quality between theory and experiment for individual RBC is illustrated by the median values of δ (bottom row in Fig. 2). The variations of median δ from donor to donor can be caused by differences between real RBC shapes and RBC optical models based on minimization of membrane bending energy (normal

RBC shape). Abnormal RBCs result in larger δ values; hence, we assume that median δ correlates with amount of normal RBC in a sample. However, this assumption requires future studies involving both confocal microscopy and scanning flow cytometry.

Such large amount of information obtained from each RBC can be visualized by distributions, two- and three-dimensional scatterplots, as well as by RBC indices statistically derived from the distributions. We showed several examples and discussed apparent features, such as presence of almost spherical cells. However, further (clinical) studies are required to establish normal bounds for new indices and correlate deviation of indices from these bounds to certain pathologies. The latter should at least include pathologies accompanied by deformation of RBC shape.

An important further research direction is enhancing the RBC shape model, for example, by accounting for cytoskeletal proteins, to also describe non-discoidal shapes (cup-shaped ones, sickle cells). This will lead to generalization of the characterization method to deal with such abnormal cells. However, such enhancement will definitely increase the number of model characteristics, requiring, in turn, improvements in optical set-up of the flow cytometer. The goal of the latter should be to increase the amount of independent light-scattering data to keep good precision of the solution of the inverse light-scattering problem.

To conclude, absence of consumables and fast analysis time make the proposed method perfect for routine clinical diagnostics, significantly increasing its descriptiveness and sensitivity to pathologies interfering with RBC characteristics. Moreover, it can be easily combined with consumable-free analysis of blood platelets (37), thus covering the two most representative cells in blood.

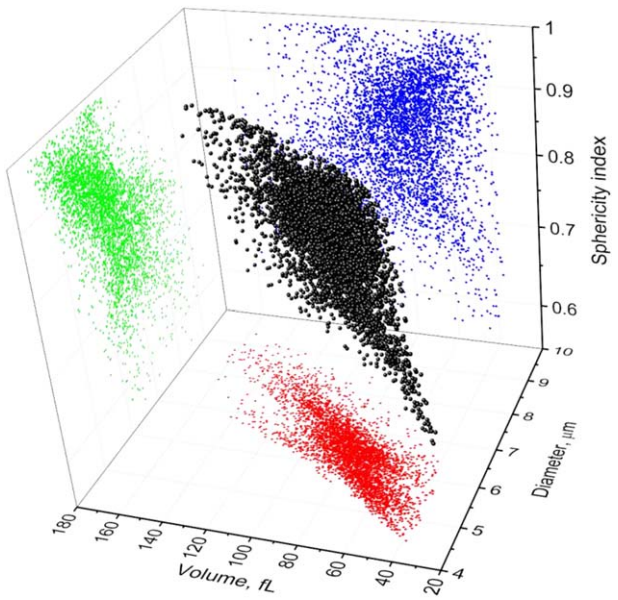

Figure 4. The 3D scatterplot with 2D projections for RBC characteristics of donor #21. [Color figure can be viewed at wileyonlinelibrary.com]

Table 2. The ranges of mean over sample RBC characteristics among all donors.

CHARACTERISTIC	MIN	AVERAGE	MAX
Diameter, μm	5.60	6.42	7.75
Min thickness, μm	1.03	1.90	2.78
Max thickness, μm	2.59	3.03	3.68
Volume, fl	57.3	77.8	117.9
Surface, μm^2	80.8	101.1	135.0
Sphericity index	0.68	0.80	0.90
Spontaneous curvature, μm^{-1}	−0.91	−0.47	−0.12
Dimensionless spontaneous curvature	−2.43	−1.27	−0.34
Hb concentration, g/dL	31.4	38.5	45.3
Hb content, pg	17.6	29.2	53.0
Median δ	0.090	0.117	0.151

Literature Cited

1. Diez-Silva M, Dao M, Han J, Lim C-T, Suresh S. Shape and biomechanical characteristics of human red blood cells in health and disease. MRS Bulletin 2010;35:382–388.
2. Engström KG, Löfvenberg E. Treatment of myeloproliferative disorders with hydroxyurea: Effects on red blood cell geometry and deformability. Blood 1998;91:3986–3991.
3. Canham PB, Burton AC. Distribution of size and shape in populations of normal human red cells. Circ Res 1968;22:405–422.
4. Bransky A, Korin N, Nemirovski Y, Dinnar U. Correlation between erythrocytes deformability and size: A study using a microchannel based cell analyzer. Microvascular Res 2007;73:7–13.
5. Gifford SC, Frank MG, Derganc J, Gabel C, Austin RH, Yoshida T, Bitensky MW. Parallel microchannel-based measurements of individual erythrocyte areas and volumes. Biophys J 2003;84:623–633.
6. Tomaiuolo G, Rossi D, Caserta S, Cesarelli M, Guido S. Comparison of two flow-based imaging methods to measure individual red blood cell area and volume. Cytometry Part A 2012;81A:1040–1047.
7. Fung Y-C, Tsang W, Patitucci P. High-resolution data on the geometry of red blood cells. Biorheology 1981;18:369–385.
8. Rappaz B, Barbul A, Emery Y, Korenstein R, Depeursinge C, Magistretti PJ, Marquet P. Comparative study of human erythrocytes by digital holographic microscopy, confocal microscopy, and impedance volume analyzer. Cytometry Part A 2008;73A:895–903.
9. Moon I, Javidi B, Yi F, Boss D, Marquet P. Automated statistical quantification of three-dimensional morphology and mean corpuscular hemoglobin of multiple red blood cells. Opt Express 2012;20:10295–10309.
10. Hayashi Y, Oshige I, Katsumoto Y, Omori S, Yasuda A, Asami K. Dielectric inspection of erythrocyte morphology. Phys Med Biol 2008;53:2553–2564.
11. Khairy K, Foo J, Howard J. Shapes of red blood cells: Comparison of 3D confocal images with the bilayer-couple model. Cellular Mol Bioeng 2008;1:173–181.
12. Mir M, Tangella K, Popescu G. Blood testing at the single cell level using quantitative phase and amplitude microscopy. Biomed Opt Express 2011;2:3259–3266.
13. Phillips KG, Jacques SL, McCarty OJT. Measurement of single cell refractive index, dry mass, volume, and density using a transillumination microscope. Phys Rev Lett 2012;109:118105.
14. Kim Y, Shim H, Kim K, Park H, Jang S, Park Y. Profiling individual human red blood cells using common-path diffraction optical tomography. Sci Rep 2014;4:6659.
15. Park Y, Diez-Silva M, Popescu G, Lykotrafitis G, Choi W, Feld MS, Suresh S. Refractive index maps and membrane dynamics of human red blood cells parasitized by Plasmodium falciparum. Proc Natl Acad Sci U S A 2008;105:13730–13735.
16. Hurley J. Sizing particles with a coulter counter. Biophys J 1970;10:74–79.
17. Tycko DH, Metz MH, Epstein EA, Grinbaum A. Flow-cytometric light scattering measurement of red blood cell volume and hemoglobin concentration. Appl Opt 1985;24:1355–1365.
18. Arnfred T, Kristensen SD, Munck V. Coulter counter model S and model S-plus measurements of mean erythrocyte volume (MCV) are influenced by the mean erythrocyte haemoglobin concentration (MCHC). Scand J Clin Lab Invest 1981;41:717–721.
19. Semyanov KA, Tarasov PA, Soini JT, Petrov AK, Maltsev VP. Calibration-free method to determine the size and hemoglobin concentration of individual red blood cells from light scattering. Appl Opt 2000;39:5884–5889.
20. Piagnerelli M, Zouaoui Boudjeltia K, Brohee D, Vereerstraeten A, Piro P, Vincent J-L, Vanhaeverbeek M. Assessment of erythrocyte shape by flow cytometry techniques. J Clin Pathol 2006;60:549–554.
21. Kubota F. Analysis of red cell and platelet morphology using an imaging-combined flow cytometer. Clin Lab Haematol 2003;25:71–76.
22. Maltsev VP. Scanning flow cytometry for individual particle analysis. Rev Sci Instrum 2000;71:243–255.

23. Strokotov DI, Moskalensky AE, Nekrasov VM, Maltsev VP. Polarized light-scattering profile-advanced characterization of nonspherical particles with scanning flow cytometry: Polarized Light Scattering. Cytometry Part A 2011;79A:570–579.
24. Strokotov DI, Yurkin MA, Gilev KV, van Bockstaele DR, Hoekstra AG, Rubtsov NB, Maltsev VP. Is there a difference between T- and B-lymphocyte morphology? J Biomed Opt 2009;14:064036.
25. Moskalensky AE, Yurkin MA, Konokhova AI, Strokotov DI, Nekrasov VM, Chernyshev AV, Tsvetovskaya GA, Chikova ED, Maltsev VP. Accurate measurement of volume and shape of resting and activated blood platelets from light scattering. J Biomed Opt 2013;18:12–017001.
26. Yurkin MA, Semyanov KA, Tarasov PA, Chernyshev AV, Hoekstra AG, Maltsev VP. Experimental and theoretical study of light scattering by individual mature red blood cells by use of scanning flow cytometry and a discrete dipole approximation. Appl Opt 2005;44:5249–5256.
27. Gilev KV, Yurkin MA, Chernyshova ES, Strokotov DI, Chernyshev AV, Maltsev VP. Mature red blood cells: from optical model to inverse light-scattering problem. Biomed Opt Express 2016;7:1305.
28. Konokhova AI, Gelash AA, Yurkin MA, Chernyshev AV, Maltsev VP. High-precision characterization of individual E. coli cell morphology by scanning flow cytometry. Cytometry Part A 2013;83A:568–575.
29. Konokhova AI, Yurkin MA, Moskalensky AE, Chernyshev AV, Tsvetovskaya GA, Chikova ED, Maltsev VP. Light-scattering flow cytometry for identification and characterization of blood microparticles. J Biomed Optics 2012;17:0570061–0570068.
30. Konokhova AI, Rodionov AA, Gilev KV, Mikhaelis IM, Strokotov DI, Moskalensky AE, Yurkin MA, Chernyshev AV, Maltsev VP. Enhanced characterisation of milk fat globules by their size, shape and refractive index with scanning flow cytometry. Int Dairy J 2014;39:316–323.
31. Konokhova AI, Chernova DN, Moskalensky AE, Strokotov DI, Yurkin MA, Chernyshev AV, Maltsev VP. Super-resolved calibration-free flow cytometric characterization of platelets and cell-derived microparticles in platelet-rich plasma: Super-resolved characterization of plasma cells. Cytometry Part A 2016;89A: 159–168.
32. Dannhauser D, Rossi D, Causa F, Memmolo P, Finizio A, Wriedt T, Hellmers J, Eremin Y, Ferraro P, Netti PA. Optical signature of erythrocytes by light scattering in microfluidic flows. Lab Chip 2015;15:3278–3285.
33. Yurkin MA, Hoekstra AG. The discrete-dipole-approximation code ADDA: Capabilities and known limitations. J Quant Spectrosc Radiat Transf 2011;112:2234–2247.
34. Bohren CF, Huffman DR. Electromagnetic Theory. In: Absorption and Scattering of Light by Small Particles. WILEY-VCH Verlag GmbH & Co. KGaA, Weinheim; 2004. p 1256.
35. Barer R, Joseph S. Refractometry of living cells: Part I. Basic principles. Q J Microsc Sci1954;95:399–423.
36. Sarma PR. Red Cell Indices. In: Walker HK, Hall WD, Hurst JW, editors Clinical Methods: The History, Physical, and Laboratory Examinations, 3rd ed. Boston: Butterworths; 1990.
37. Litvinenko A. l, Moskalensky AE, Karmadonova NA, Nekrasov VM, Strokotov DI, Konokhova AI, Yurkin MA, Pokushalov EA, Chernyshev AV, Maltsev VP. Fluorescence-free flow cytometry for measurement of shape index distribution of resting, partially activated, and fully activated platelets. Cytometry Part A 2016;89A: 1010–1016.